LANGMUIR

Article

pubs.acs.org/Langmuir

Complex Filling Dynamics in Mesoporous Thin Films

Magalí Mercuri,[†] Karina Pierpauli,[†] Martín G. Bellino,*[,†] and Claudio L. A. Berli*[,‡]

[†]Departamento de Micro y Nanotecnología, Comisión Nacional de Energía Atómica, Avenida General Paz 1499, San Martín, B1650 Buenos Aires, Argentina

[‡]INTEC (Universidad Nacional del Litoral-CONICET) Predio CCT CONICET Santa Fe, RN 168, S3000 Santa Fe, Argentina

Supporting Information

ABSTRACT: The fluid-front dynamics resulting from the coexisting infiltration and evaporation phenomena in nanofluidic systems has been investigated. More precisely, water infiltration in both titania and silica mesoporous films was studied through a simple experiment: a sessile drop was deposited over the film and the advancement of the fluid front into the porous structure was optically followed and recorded in time. In the case of titania mesoporous films, capillary infiltration was arrested at a given distance, and a steady annular region of the wetted material was formed. A simple model that combines Lucas−Washburn infiltration and surface evaporation was derived, which appropriately describes the observed filling dynamics and the annulus width in dissimilar mesoporous morphologies. In the case of wormlike mesoporous morphologies, a remarkable phenomenon was found: instead of reaching a steady infiltration−evaporation balance, the fluid front exhibits an oscillating behavior. This complex filling dynamics opens interesting possibilities to study the unusual nanofluidic phenomena and to discover novel applications.

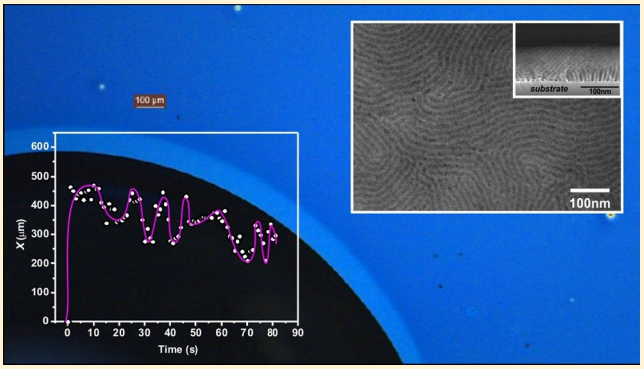

INTRODUCTION

One issue of rising interest is the spontaneous imbibition of fluids in structures with nanoscale morphology. Three-dimensional nanoporous networks find applications in technologies such as catalysis,[1] sorption,[2] filtration,[3] sensing,[4] and optical switches.[5] Mesoporous films are modular and scalable from miniaturization of devices to large area integration with matter.[6,7] Indeed, the confined space of the mesoporous films offers unbeatable opportunities for the study of novel fluid behavior in nanoconduits.[8] In these systems, capillarity has been shown to drive the wetting liquid infiltration, constituting a natural way to propel nanoflows. Even for nanoscale pores, theories and experiments confirm the classic Lucas−Washburn law, which predicts a square-root of time imbibition kinematics.[9−12] Nevertheless, water infiltration in mesoporous thin films is strongly influenced by evaporation, and hence, the kinematics is different to that generally found for the conventional porous materials. Actually, the dynamics of liquid−vapor interfaces in nanofluidic systems is still poorly understood, in contrast to its important role in nature and technological applications.[13,14]

In this context, the present study deals with the following experimental problem: a sessile drop deposited over a mesoporous film exhibits an annular region of the wetted material formed by the arrested capillary infiltration. The phenomenon has been illustrated in detail in a recent work,[8] where the balance between capillary filling from the liquid drop and surface evaporation to the environment is considered, however, without quantitative descriptions. On the other hand, a model for the radial capillary filling of porous substrates limited by evaporation has been lately reported,[15] without experimental results. Here, the problem is discussed by means of both theories and experiments. A phenomenological model that combines Lucas−Washburn infiltration and surface evaporation is used, which appropriately describes the filling dynamics observed in titania films with dissimilar mesoporous morphologies. Furthermore, it is found that the silica mesoporous films with wormlike nanostructures, instead of maintaining a steady infiltration−evaporation balance, exhibit an oscillating behavior of the liquid−vapor interface. This complex phenomenon has not been reported before, to the best of our knowledge, and opens several attractive possibilities in interface science and technology.

The article is organized as follows. The material and methods used in the sample characterization are presented in the following section, and the formulation of the model is described in the subsequent section. Then, the experimental results are discussed together with the model-based interpretation, and a novel complex behavior found during water infiltration in mesoporous films is presented. Finally, some concluding remarks are outlined.

Received: November 3, 2016
Revised: December 12, 2016
Published: December 13, 2016

DOI: 10.1021/acs.langmuir.6b03987
Langmuir 2017, 33, 152−157

EXPERIMENTAL SECTION

Film Synthesis. Crack-free mesoporous titania and silica films were deposited by dip-coating a supramolecularly templated oxide precursor.[16] The use of Pluronics F127 as a surfactant and different thermal treatments allow dissimilar mesoporous morphology to be obtained after the template removal.[17] The technique is based on the evaporation-induced self-assembly strategy using an inorganic precursor and a surfactant template in ethanol solution. Three types of porous morphologies were used for this study. Mesoporous TiO_2 films with locally ordered mesostructures (MPO) were prepared using the standard consolidation−calcination steps. TiO_2 conduit-like mesostructures (MCL) presenting domains of aligned pores and SiO_2 wormlike mesostructures (MWL) were obtained by a fast-firing thermal treatment. Mesoporous titania thin films were dip-coated at 3 mm/s on silicon substrates at a relative humidity (RH) of 30%, and silica films were deposited on silicon at 1.5 mm/s. $TiCl_4$ and $Si(OEt)_4$ were used as inorganic precursors for titania and silica films, respectively, and Pluronics F127 was selected as the polymeric template. MPO and MCL initial solutions were composed of a $TiCl_4$/EtOH/H_2O/F127 mixture, with a 1:40:10:0.005 ratio of the reagents, whereas MWL final molar ratios were 1:40:5:0.04 for the mixture tetraethyl orthosilicate/EtOH/H_2O/F127. After deposition, the MPO films were placed in 50% RH chambers overnight. The films were then subjected to a consolidation thermal treatment, which consisted of heating for 2 h at 60 °C and then 2 h at 130 °C, and finally were calcined at 450 °C for 2 h to remove the templating agent; the temperature ramp was 1 °C/min. In the case of MCL and MWL samples, the films were directly calcined in the absence of the consolidation steps by a fast-firing process, with a dwell temperature of 450 °C and a dwell time of 10 min.

Film Characterization. H_2O-adsorption isotherms with pore size distributions were measured by environmental ellipsometric porosimetry (EEP).[18] Film thickness and reflective index n values were obtained from the ellipsometric parameters ψ and Δ at each P/P_0 (P_0 being the saturation water pressure), which was varied from 0 to 1 using a SOPRA GES5A ellipsometer. Film porosity ϕ was evaluated using the WinElli 2 software (SopraInc), which transforms the variation of n with P/P_0 into a filled pore volume by using a three-medium Bruggeman effective medium approximation treatment. Pore and pore neck size distributions were derived according to a Kelvin model. Pore neck (also called throat) represents the interconnection between the pores. More details on the EEP technique are given in the Supporting Information. Micrographs were obtained using a Zeiss LEO 982 Gemini field-emission electron microscope in the secondary-electron mode, using an in-lens detector to improve resolution. Transmission electron images were taken using a Philips CM200 electron microscope. The contact angle of sessile water drops was measured by using a Ramé-Hart goniometer, taking an average of three measurements taken at different sites of each sample.

Infiltration Measurements. Water infiltration into the mesoporous films from a 2 μL sessile drop was followed by using a Leica DM 2700M optical microscope at 23 °C and 46% RH. Images were recorded using a high-resolution digital camera. Image data were analyzed using the *Tracker* software (Open Source Physics; Java framework). The reported fluid-front distances versus time data correspond to an average of 10 measurements taken at different positions along the drop perimeter. Control experiments were performed using the substrate (silicon) in the absence of the mesoporous film, where no annulus was observed.

THEORY

In this section, we derive a phenomenological model for the dynamics of the water infiltration−evaporation in mesoporous films, to describe the annular region of the wetted material formed around a sessile drop. The annulus can be clearly seen in Figure 1a, where the wetted region produces a refractive index contrast in relation to the outer dry zone. For the sake of simplicity, the filling dynamics is modeled by using a one-dimensional flow domain, as shown schematically in Figure 1b. The approach is valid for the system under study because the drop radius is much larger than the annulus width; hence, the imbibition front can be considered to be locally flat.

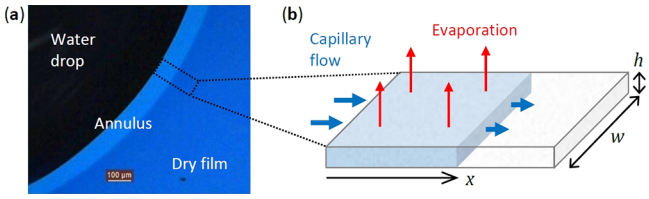

Figure 1. (a) Typical top-view microscope image of the water droplet deposited on the mesoporous film showing the infiltrated annular region. (b) Flow domain geometry and schematic representation of the transport processes considered in modeling.

Experiments reported elsewhere[8] show that, when evaporation is minimized, the capillary-driven infiltration in mesoporous films follows the classical Lucas−Washburn kinematics.[19,20] Thus, for a generic porous domain with a uniform cross section, the infiltration rate can be written as[21]

$$\left.\frac{dx}{dt}\right|_{LW} = \frac{c}{x} \tag{1}$$

where x is the position of the imbibition front at time t. Also, in this expression, $c = k\Delta p/\mu\phi$ is the dynamic coefficient, where k is the matrix permeability, Δp is the Laplace pressure, and μ is the fluid viscosity. The simplest microstructural model for the permeability of the porous matrix is that of the cylindrical nanopores of radius r aligned in the flow direction, for which $k = r^2/8$.[11,20]

To take into account the mass loss due to the evaporation of the test liquid, here we assume that the evaporation rate per unit area of the wetted surface (A_{ev}) is constant for a given liquid, air temperature, and relative saturation of the environment[22]

$$\dot{m}_{ev} = \frac{1}{A_{ev}}\frac{dm}{dt} \tag{2}$$

Therefore, the one-dimensional variation in the control volume due to evaporation can be expressed as

$$\left.\frac{dx}{dt}\right|_{ev} = -\frac{\dot{m}_{ev}x}{h\rho\phi} \tag{3}$$

where ρ is the fluid density. This expression includes the hypothesis that evaporation takes place on the surface $A_{ev} = wx$, as the lower side of the film is isolated and $h \ll x$. In fact, the experimental observations of position x are made within intervals of some micrometers, whereas the film thickness is 180 nm (see Table 1 for mesoporous films structural data).

Although evaporation produces heat exchange, which is particularly effective in thin films, here the flow domain is considered to be isothermal, as a first approximation. Under these conditions, the overall fluid-front velocity is obtained by

Table 1. Structural Data of the Mesoporous Titania Thin Films

sample	pore size (nm)	neck size (nm)	film thickness h (nm)	porosity ϕ (%)
MPO	12	4.5	180	45
MCL	6	4.1	180	50

DOI: 10.1021/acs.langmuir.6b03987
Langmuir 2017, 33, 152−157

adding the rate of the processes described above, which leads to the following differential equation

$$\frac{dx}{dt} = \frac{c}{x} - \frac{x}{\tau} \tag{4}$$

where the characteristic evaporation time τ is defined as follows

$$\tau = \frac{h\rho\phi}{\dot{m}_{ev}} \tag{5}$$

Equation 4 coincides with expressions recently reported to model capillary infiltration in the presence of evaporation for a range of porous media (such as walls,[23] metallic weaves,[24] and nanowire network films[25]). It is observed in eq 4 that the first term predominates at short distances/times, whereas the second one takes relevance at longer distances/times. Therefore, there is a position x where the processes balance ($dx/dt = 0$) and the fluid front reaches the steady-state position

$$x_{ss} = (c\tau)^{1/2} \tag{6}$$

This simple result has relevant meanings: the prediction of an annulus width x_{ss} defined by the competition between the infiltration and the evaporation processes, the functional dependence of x_{ss} on c and τ, and the possibility to extract the valuable information on the system from a simple distance measurement.

The kinematics of the infiltration−evaporation process can be readily obtained by integrating eq 4 with the initial condition $t = 0$, $x = 0$

$$x^2(t) = x_{ss}^2[1 - \exp(-2t/\tau)] \tag{7}$$

Equation 7 represents the squared time-dependent position of the fluid front; more precisely, $x(t)$ is the time-dependent width of the annular wetted region. Figure 2 illustrates the prediction of eq 7 for different parameter values. At very short times ($t \ll \tau$), $x^2(t)$ has a linear growth corresponding to the Lucas−Washburn regime. At very long times ($t \gg \tau$), $x^2(t)$ asymptotically reaches the constant value x_{ss}^2. For intermediate stages, the rate of the process is controlled by the characteristic time τ. Figure 2 also shows how the steady-state annulus width

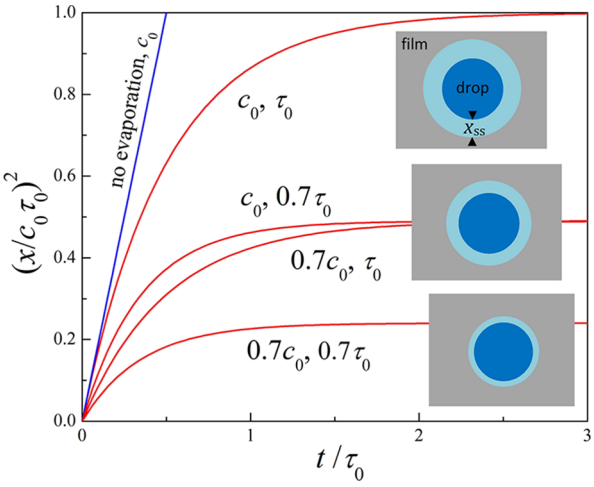

Figure 2. Squared position of the infiltration front as a function of time, made dimensionless with arbitrary values of c_0 and τ_0. The curves correspond to different parameter values, written as variations in c_0 and τ_0. The insets are schematic drawings to show the steady-state annulus width expected in each case (not to scale).

is determined by the combination of both c and τ, as indicated in eq 6. For a more practical interpretation, it should be taken into account that decreasing τ means increasing the evaporation rate $\dot{m}_{ev}$, whereas decreasing c means increasing the hydrodynamic resistance of the porous matrix. Of course, for relatively large $\dot{m}_{ev}$, the annulus width will be negligibly small.

RESULTS AND DISCUSSION

Characteristics of Mesoporous Films. Figure 3 presents the typical scanning electron microscopy (SEM) and transmission electron microscopy (TEM) micrographs showing the mesoporous structures of the studied films: MPO and mesostructures presenting domains of aligned pores (MCL). H_2O-adsorption isotherms with pore size distributions measured by EEP for the MPO and MCL samples are shown in Figure S1. The structural characteristics of these films are summarized in Table 1. Pore dimensions obtained by EEP are in agreement with the electron microscopy images. The contact angles of sessile water drops over the films were 53° and 61° for

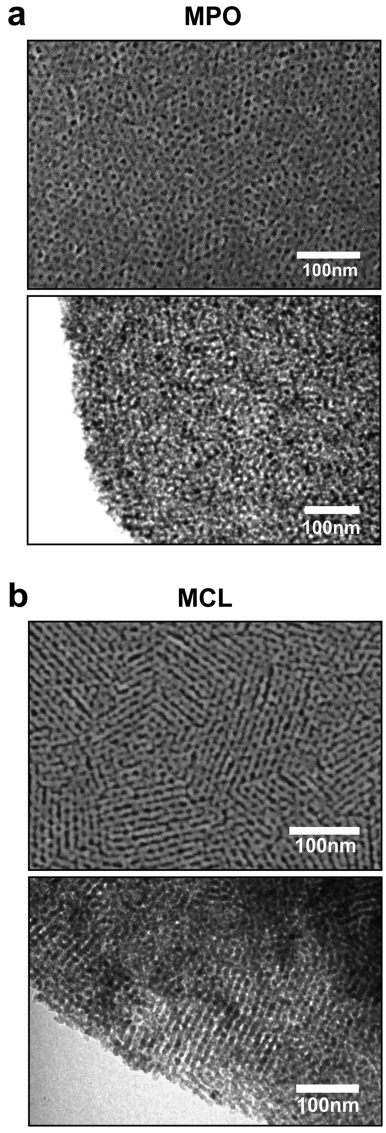

Figure 3. Mesoporous film characterization: SEM (top) and TEM (bottom) micrographs of MPO (a) and MCL (b) samples.

DOI: 10.1021/acs.langmuir.6b03987
Langmuir 2017, 33, 152−157

MPO and MCL, respectively (the surface tension of water at room temperature is γ = 72 mM/m).

Infiltration Experiments in Titania Films. Dynamic nanofluidic experiments were carried out by recording the evolution of the annular wetted region as a function of time. Typical curves of the squared position of the fluid front are shown in Figure 4. A steady-state position of the fluid front is

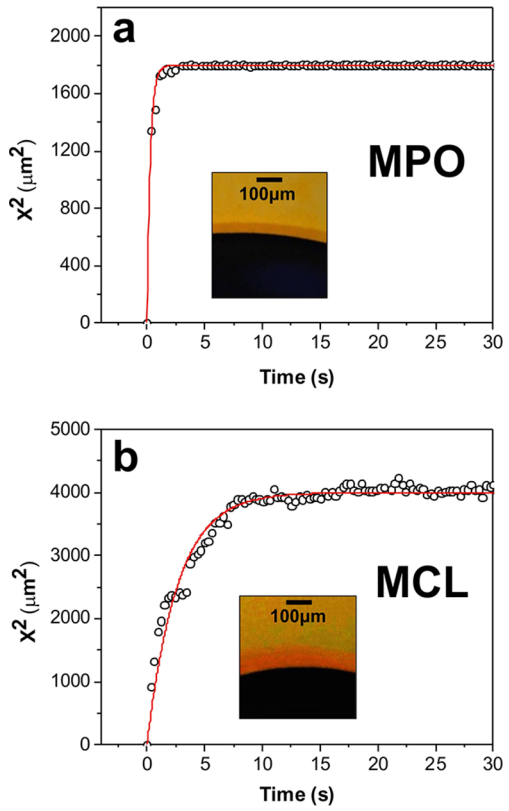

Figure 4. Squared position of the fluid front as a function of time for (a) MPO and (b) MCL samples. Symbols represent the experimental data and lines are the prediction of eq 7 with respect to the parameters x_{ss} and τ reported in Table 2. The insets show images of the steady-state width of the annulus surrounding the sessile water drop in the respective experiments.

observed, as predicted by eq 6. This arrest of the infiltration is not usually found in the conventional porous materials, where evaporation have negligible effects and capillary filling expands the whole sample (provided the drop volume is high enough). Regarding the dynamics of the process, one may observe in Figure 4 that the infiltration presents two main stages: the instantaneous response of the fluid to the capillary action (much faster than evaporation) and the slower, longer-range fluid evaporation that occurs over a larger time scale. This behavior exhibits the relevant effects of evaporation on the nanofluidic transport in mesoporous films.

The solid lines in Figure 4 are the predictions of eq 7 for the respective values of x_{ss} and τ (fitting parameters), as reported in Table 2. One may observe that the phenomenological model satisfactorily describe infiltration in the mesoporous films with quite dissimilar nanostructures. The values of constant c reported in Table 2 were calculated using eq 6 with data of x_{ss} and τ. In the case of MPO, c compares well with that of the similar mesoporous films reported in the literature: for instance, the samples synthetized with Pluronics F127 as a surfactant

Table 2. Fitting Parameters x_{ss} and τ from the Curves (eq 7) Plotted in Figure 4, Dynamic Coefficient c Calculated from eq 6, and Evaporation Rate $\dot{m}_{ev}$ Calculated from eq 5

sample	x_{ss} (μm)	τ (s)	c (μm^2/s)	$\dot{m}_{ev}$ kg/(m^2 s)
MPO	42	0.6	3046	1.4×10^{-4}
MCL	63	5.3	755	1.7×10^{-5}

reported in ref 8 present c values between 6400 and 14 000 μm^2/s. By contrast, the MCL sample presents a much lower values of c. This relatively high hydrodynamic resistance may be attributed to the tortuous conduit-like structure observed in the SEM micrographs of the film.

The values of $\dot{m}_{ev}$ presented in Table 2 were calculated using eq 5, with values of τ from the same table, data of h and ϕ reported in Table 1, and fluid density $\rho = 10^3$ kg/m^3. The resulting evaporation rate for the MPO film is in very good agreement with the values reported for the nanostructured films (1.2×10^{-4} kg/(m^2 s) in ref 25), as well as with those found in drying experiments of rigid porous materials ($1-7 \times 10^{-4}$ kg/(m^2 s) in ref 26). The lower evaporation rate resulting in MCL films is reasonable, taking into account the confinement effects due to the smaller pore sizes. Finally, it is interesting to observe in Figure 4 the interplay of c and τ that leads to the overall response: MPO permeability is around 4 times higher than that of MCL; however, the largest annulus is observed in MCL, owing to its significantly lower evaporation rate.

Complex Behavior in Silica Films. Silica films present wormlike mesostructures, as shown in the micrographs of Figure 5 (top panel). One may infer that these open structures, presenting rather continuous tracks for fluid motion in the film plane, would produce larger imbibition distances in comparison

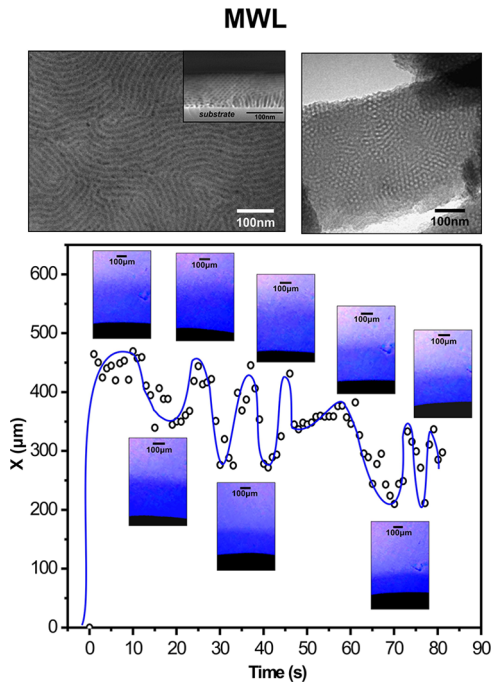

Figure 5. Structural characterization and nanofluidic behavior of the MWL sample. Top images: SEM (left) and TEM (right) micrographs; the inset in the SEM image shows a profile cut. Bottom graphic: fluid-front distance as a function of time. The symbols are the experimental data, and the solid line is a guide for the eye. Inset pictures illustrate the oscillating behavior at the respective times (see Movie S1).

DOI: 10.1021/acs.langmuir.6b03987
Langmuir 2017, 33, 152−157

with the titania films. A lower contact angle of sessile water drops was also observed: 24° for the MWL sample. Effectively, once the water drop is deposited on the film, a very fast infiltration is observed and the fluid front suddenly expands almost 500 μm. Nevertheless, instead of asymptotically reaching a steady-state position, the fluid front displays an oscillatory movement, uniformly around the liquid drop, with amplitude around 100 μm and oscillating period around 12 s, as shown in Figure 5. This remarkable phenomenon can be vividly observed in the videos taken during experiments (see Movie S1).

The oscillatory behavior of the liquid−vapor interface would be a consequence of a time-dependent imbalance between infiltration and evaporation. We were unable to find reports on such behavior in the literature nor a rational explanation at present. In what follows, we will mention some particular features of the MWL sample and then some conjectures to open the discussion.

The sol−gel process yields two main geometry scales (pores and pore-necks), each one with some size distribution, as it is evidenced in the bell-shaped curves obtained from adsorption−desorption isotherms (see Figure S1). This pore size distribution would promote broadening of the fluid front, which however moves following the Lucas−Washburn dynamics.[27] Furthermore, it has been just reported[28] that, for relatively short pores, neighboring menisci form a rather homogenous infiltration front. This is likely the case of MPO and MCL samples, which exhibited a quite net liquid−air interface in infiltration experiments (see images in Figures 1 and 4), and then a steady annulus was formed. On the other hand, the front broadening effect is much more pronounced in systems where the pores are elongated and independent of each other,[28] such as the wormlike structures observed in the MWL samples. Furthermore, it is also possible that the wetted area where oscillations take place is precisely the broaden front, which quickly expands after the droplet is laid over the film. If that were the case, the system would have a different characteristic time and a position-dependent evaporation rate (because of the average water density variation in the film surface). These features would add complexity to the problem, but they do not necessarily entail a possible mechanism for the oscillations, which requires the presence of a restoring driving force or some bivalued phase diagram. Of course, further experiments need to be performed to clarify these aspects.

Up to this point, we have considered the problem to be isothermal. Nevertheless, a raw speculation is that the (sort of) instability in the fluid-front position may be originated by a sudden temperature change during the evaporation stage. Actually, the porous films are well-known to produce substantial cooling rates by the evaporation of the wetted fluids.[29] A sudden temperature decrease from 25 to 15 °C would yield around 20% diminution of c only because of the viscosity variation (note that surface tension γ, which enters c through the capillary pressure Δp, also depends on temperature). In Figure 2, it is equivalent to jump dawn from the curve of $c = c_0$ to one with $c = 0.8c_0$. The associated variation in x_{ss} is fairly in the order of the relative amplitude of the oscillations observed in Figure 5. Given this interplay, a subsequent increase in the local temperature (toward room temperature value) would drive a further advancement of the fluid front and then the resultant cycling.

Exploring this hypothesis by theory requires studying the coupling of fluid momentum, mass transport, and heat transfer in the nanofluidic system, which constitutes a demanding problem that needs further research. Of course, a more insightful understanding of evaporation at small scales has to be included,[30] as well as the consideration of vapor water and biphasic flows.[31] In any case, the observation of a periodic forward and backward displacement of the fluid front is another remarkable indication of the complex behavior of fluids in the mesoporous films.

SUMMARY AND CONCLUSIONS

In summary, this study provides strong evidence that the infiltration dynamics in mesoporous thin films largely reflects the time course of evaporation rather than the filling rate. Both the experimental and the theoretical model demonstrate that evaporation plays a key role in controlling the nanoscale transport processes in MPO and MCL films. Taking into consideration that the experimental curves are very sensitive to the dissimilar morphology of the mesoporous films, next step in modeling is the connection of transport properties to pore sizes and architecture (an attempt on dynamic coefficient c has just been published[32]), to have a valuable tool to characterize the film nanostructures from simple fluidic experiments, as well as to modulate the transport properties of the mesoporous films during their synthesis.

On the other hand, the remarkable oscillatory behavior found in MWL films opens interesting possibilities in two ways: from the point of view of fundamentals, finding a thorough description of the complex dynamics exhibited by the liquid−vapor interface is a challenging problem that undoubtedly motivates further investigation; from a technological point of view, studying unusual nanofluidic phenomena and discovering novel ultrafast platforms could provide clues to design new operations in microdevices.

ASSOCIATED CONTENT

Supporting Information

The Supporting Information is available free of charge on the ACS Publications website at DOI: 10.1021/acs.langmuir.6b03987.

Sample characterization by environmental ellipsometric porosimetry (PDF)

Oscillating behavior of the fluid front around a sessile water drop deposited on a silica mesoporous film (AVI)

AUTHOR INFORMATION

Corresponding Authors

*E-mail: mbellino@cnea.gov.ar (M.G.B.).

*E-mail: cberli@santafe-conicet.gov.ar (C.L.A.B.).

ORCID

Claudio L. A. Berli: 0000-0002-1321-6738

Notes

The authors declare no competing financial interest.

ACKNOWLEDGMENTS

M.M. acknowledges the doctoral fellowship from CNEA, Argentina. This work was supported by CONICET (PIP-0363) and ANPCyT (PICT-2015-1051 and PICT-2012-2969), Argentina.

DOI: 10.1021/acs.langmuir.6b03987
Langmuir 2017, 33, 152−157

REFERENCES

(1) Tanev, P. T.; Chibwe, M.; Pinnavaia, T. J. Titanium-containing mesoporous molecular sieves for catalytic oxidation of aromatic compounds. *Nature* **1994**, *368*, 321−323.

(2) Kresge, C. T.; Leonowicz, M. E.; Roth, W. J.; Vartuli, J. C.; Beck, J. S. Ordered mesoporous molecular sieves synthesized by a liquid-crystal template mechanism. *Nature* **1992**, *359*, 710−712.

(3) Kim, Y.; Kim, C.; Choi, I.; Rengaraj, S.; Yi, J. Arsenic removal using mesoporous alumina prepared via a templating method. *Environ. Sci. Technol.* **2004**, *38*, 924−931.

(4) Slowing, I. I.; Trewyn, B. G.; Giri, S.; Lin, V. S.-Y. Mesoporous silica nanoparticles for drug delivery and biosensing applications. *Adv. Funct. Mater.* **2007**, *17*, 1225−1236.

(5) Kalyanasundaram, K.; Grätzel, M. Applications of functionalized transition metal complexes in photonic and optoelectronic devices. *Coord. Chem. Rev.* **1998**, *177*, 347−414.

(6) Sanchez, C.; Boissière, C.; Grosso, D.; Laberty, C.; Nicole, L. Design, synthesis, and properties of inorganic and hybrid thin films having periodically organized nanoporosity. *Chem. Mater.* **2008**, *20*, 682−737.

(7) Innocenzi, P.; Malfatti, L. Mesoporous thin films: Properties and applications. *Chem. Soc. Rev.* **2013**, *42*, 4198−4216.

(8) Ceratti, D. R.; Faustini, M.; Sinturel, C.; Vayer, M.; Dahirel, V.; Jardat, M.; Grosso, D. Critical effect of pore characteristics on capillary infiltration in mesoporous films. *Nanoscale* **2015**, *7*, 5371−5382.

(9) Dimitrov, D. I.; Milchev, A.; Binder, K. Capillary rise in nanopores: Molecular dynamics evidence for the Lucas−Washburn equation. *Phys. Rev. Lett.* **2007**, *99*, 054501.

(10) Gruener, S.; Huber, P. Imbibition in mesoporous silica: Rheological concepts and experiments on water and a liquid crystal. *J. Phys.: Condens. Matter* **2011**, *23*, 184109.

(11) Acquaroli, L. N.; Urteaga, R.; Berli, C. L. A.; Koropecki, R. R. Capillary filling in nanostructured porous silicon. *Langmuir* **2011**, *27*, 2067−2072.

(12) Xue, Y.; Markmann, J.; Duan, H.; Weissmüller, J.; Huber, P. Switchable imbibition in nanoporous gold. *Nat. Commun.* **2014**, *5*, 4237.

(13) Lee, J.; Laoui, T.; Karnik, R. Nanofluidic transport governed by the liquid/vapour interface. *Nat. Nanotechnol.* **2014**, *9*, 317−323.

(14) Huber, P. Soft matter in hard confinement: Phase transition thermodynamics, structure, texture, diffusion and flow in nanoporous media. *J. Phys.: Condens. Matter* **2015**, *27*, 103102.

(15) Liu, M.; Wu, J.; Gan, Y.; Hanaor, D. A. H.; Chen, C. Q. Evaporation limited radial capillary penetration in porous media. *Langmuir* **2016**, *32*, 9899−9904.

(16) Soler-Illia, G. J. A. A.; Angelomé, P. C.; Fuertes, M. C.; Calvo, A.; Wolosiuk, A.; Zelcer, A.; Bellino, M. G.; Martínez, E. D. Mesoporous hybrid and nanocomposite thin films. A sol−gel toolbox to create nanoconfined systems with localized chemical properties. *J. Sol-Gel Sci. Technol.* **2011**, *57*, 299−312.

(17) Soler-Illia, G. J. A. A.; Angelomé, P. C.; Fuertes, M. C.; Grosso, D.; Boissiere, C. Critical aspects in the production of periodically ordered mesoporous titania thin films. *Nanoscale* **2012**, *4*, 2549−2566.

(18) Boissiere, C.; Grosso, D.; Lepoutre, S.; Nicole, L.; Bruneau, A. B.; Sánchez, C. Porosity and Mechanical Properties of Mesoporous Thin Films Assessed by Environmental Ellipsometric Porosimetry. *Langmuir* **2005**, *21*, 12362−12371.

(19) Lucas, R. Ueber das Zeitgesetz des kapillaren Aufstiegs von Flüssigkeiten. *Kolloid-Z.* **1918**, *23*, 15−22.

(20) Washburn, E. W. The dynamics of capillary flow. *Phys. Rev* **1921**, *17*, 273−283.

(21) Elizalde, E.; Urteaga, R.; Berli, C. L. A. Rational design of capillary-driven flows for paper-based microfluidics. *Lab Chip* **2015**, *15*, 2173−2180.

(22) Scherer, G. W. Theory of drying. *J. Am. Ceram. Soc.* **1990**, *73*, 3−14.

(23) Hall, C.; Hoff, W. D. Rising damp: Capillary rise dynamics in walls. *Proc. R. Soc. A* **2007**, *463*, 1871−1884.

(24) Fries, N.; Odic, K.; Conrath, M.; Dreyer, M. The effect of evaporation on the wicking of liquids into a metallic weave. *J. Colloid Interface Sci.* **2008**, *321*, 118−129.

(25) Rogacs, A.; Steinbrenner, J. E.; Rowlette, J. A.; Weisse, J. M.; Zheng, X. L.; Goodson, K. E. Characterization of the wettability of thin nanostructured films in the presence of evaporation. *J. Colloid Interface Sci.* **2010**, *349*, 354−360.

(26) Prime, N.; Housni, Z.; Fraikin, L.; Léonard, A.; Charlier, R.; Levasseur, S. On water transfer and hydraulic connection layer during the convective drying of rigid porous material. *Transp. Porous Media* **2015**, *106*, 47−72.

(27) Gruener, S.; Sadjadi, Z.; Hermes, H. E.; Kityk, A. V.; Knorr, K.; Egelhaaf, S. U.; Rieger, H.; Huber, P. Anomalous front broadening during spontaneous imbibition in a matrix with elongated pores. *Proc. Natl. Acad. Sci. U.S.A.* **2012**, *109*, 10245−10250.

(28) Gruener, S.; Hermes, H. E.; Schillinger, B.; Egelhaaf, S. U.; Huber, P. Capillary rise dynamics of liquid hydrocarbons in mesoporous silica as explored by gravimetry, optical and neutron imaging: Nano-rheology and determination of pore size distributions from the shape of imbibition fronts. *Colloids Surf., A* **2016**, *496*, 13−27.

(29) Plawsky, J. L.; Fedorov, A. G.; Garimella, S. V.; Ma, H. B.; Maroo, S. C.; Chen, L.; Nam, Y. Nano- and microstructures for thin-film evaporation—A review. *Nanoscale Microscale Thermophys. Eng.* **2014**, *18*, 251−269.

(30) Lu, Z.; Narayanan, S.; Wang, E. N. Modeling of evaporation from nanopores with nonequilibrium and nonlocal effects. *Langmuir* **2015**, *31*, 9817−9824.

(31) Lei, W.; Fong, N.; Yin, Y.; Svehla, M.; McKenzie, D. R. Science of water leaks: Validated theory for moisture flow in microchannels and nanochannels. *Langmuir* **2015**, *31*, 11740−11747.

(32) Berli, C. L. A.; Mercuri, M.; Bellino, M. Modeling the abnormally slow infiltration rate in mesoporous films. *Phys. Chem. Chem. Phys.* **2016**, DOI: 10.1039/C6CP06602J.

DOI: 10.1021/acs.langmuir.6b03987
Langmuir 2017, 33, 152−157